Journal of The Electrochemical Society, **156** (1) C45-C53 (2009)
0013-4651/2008/156(1)/C45/9/$23.00 © The Electrochemical Society

Properties of the Nanoporous Anodic Oxide Electrochemically Grown on Steel in Hot 50% NaOH

T. D. Burleigh,[a,*,z] P. Schmuki,[b,*] and S. Virtanen[b,*]

[a]*Materials and Metallurgical Engineering Department, New Mexico Tech, Socorro, New Mexico 87801, USA*
[b]*Department of Materials Science, University of Erlangen-Nuremberg, D-91058 Erlangen, Germany*

The anodic oxide grown on steel in 50% NaOH at different temperatures and applied potentials has many remarkable properties. Optically the appearance of the oxide can vary from black to dichroic, to a light brown color. Field-effect scanning electron microscopy and X-ray diffraction reveal the oxide to be a nanoporous oxide composed of a network of 100 nm diam magnetite channels. Electrochemically the oxide is a very good conductor and, when polarized cathodic or anodic, can absorb charge by switching between Fe^{+2} and Fe^{+3}. Although the film provides excellent corrosion resistance in pure water, it provides only temporary resistance to corrosion in oxygenated saltwater. Different methods were used to seal the porous oxide, and it was found possible to reduce the corrosion rate by 2 orders of magnitude in oxygenated 0.1% NaCl solution by penetrating the oxide with a commercial inhibiting oil spray.
 [DOI: 10.1149/1.3021029]

Manuscript submitted June 25, 2008; revised manuscript received October 6, 2008. Published November 18, 2008.

Anodization of metals is an old and relatively simple method to functionalize material surfaces, by electrochemically growing a metal oxide film on the surface. For valve metals such as Al, Ti, Ta, or Zr, anodization has been extensively explored and, by a controlled variation of the electrochemical parameters used, the thickness, morphology (e.g., compact or porous layers), or crystal structure of the anodic films can be tailored to achieve the desired functionality. As for the valve metals, high voltages can be applied without substantial oxygen evolution reaction (OER) and thick anodic oxide layers can be grown before dielectric breakdown occurs. However, in the case of iron or steel, strong oxygen evolution at high anodic potentials takes place and, hence, the potential regime of oxide growth is limited.

As has been reported previously by Burleigh, in spite of oxygen evolution (and, hence, lower current efficiency), thick anodic oxide layers can be grown on steel in hot, concentrated caustic solutions in the transpassive region.[1] The present article presents a continuation of the previous work, with the aim to understand the growth mechanisms, to analyze and optimize different properties of the anodic oxide layer, and to explore the use of the anodic layer for corrosion protection of steel. This is a relatively new field of research even though there have been many diverse studies on the electrochemical behavior of steel in caustic solutions. For example, previous studies include the dissolution and passivation of iron and steel (e.g., Ref. 2-6), the production of ferrate (VI) compounds (e.g., Ref. 7 and 8), and the iron-nickel battery (e.g., Ref. 9 and 10). Only a few studies have described the use of hot caustic solutions to grow protective iron oxides on steel.[1,11-14] Burleigh has shown that when steel was polarized in the transpassive region, the applied electric current promoted the growth of a magnetite (Fe_3O_4) film in addition to oxygen evolution and iron dissolution.[1] This magnetite film has many different optical appearances, including black, dichroic, and a light brown color, depending on the temperature and the applied potential. The term "dichroic" refers to a surface that reflects different colors when viewed at different angles. This current report describes the properties of the anodic oxides grown on 1010 steel in hot 50% NaOH solution. In addition to electrochemical techniques, this paper also combines the results from a high-resolution field-effect scanning electron microscope (FESEM), X-ray diffraction (XRD), and X-ray photoelectron spectroscopy (XPS).

* Electrochemical Society Active Member.
[z] E-mail: burleigh@nmt.edu

Experimental

For the anodization, the electrolyte was 50% W/V NaOH solution (12.5 M NaOH), manufactured by Ricca Chemical Company, Arlington, Texas (500 g NaOH slowly dissolved into distilled water to make 1 L of solution). The material to be anodized was a smooth-finished, cold-rolled steel sheet, 0.25 mm thick, type-D Q-panels from Q-Lab Corporation, Westlake, Ohio. The panels were used in the as-received, cold-rolled surface condition, and prior to testing, they were degreased by wiping first with acetone and then with ethanol. The steel alloy designation was UNS G10100, with a composition (in weight percent) Fe–0.09C–0.33Mn–0.01Cu–0.01Ni–0.02Cr–0.05Al.

The anodizing temperatures were 30, 50, 70, and 90°C. The potentials were applied using a TecNu DCa 25/12-1Z power supply, which is a two-electrode system. The voltages applied were from +1.6 to + 2.6 V in 0.1 V steps vs a steel counter electrode. The to-be-anodized steel panel was placed parallel to an identical steel counter electrode/cathode at 7 cm spacing, and the solution was stirred rapidly with a magnetic stir bar in order to remove oxygen bubbles from the anodic surface and provide a uniform oxide color. The electrode spacing was important because the voltage drop across the solution affected the potential experienced by the anode. During the anodization, the anode potential was additionally measured vs the Ag_2O/20% KOH reference electrode. Although both the reference electrode and the counter electrode potentials were measured, the potentials herein are predominantly reported vs the steel counter electrode because the reference electrode potential often drifted ± 10 mV during the 5 min of anodization. After anodization, the samples were rinsed in distilled water and then dried under a stream of compressed air.

A separate steel panel was anodized for 5 min at each temperature and potential. The anodization was started with a clear solution of 50% NaOH at 30, 50, and 70°C, and the same solution was used for each sample as the voltage was increased from +1.6 to + 2.6 V vs the steel cathode. (The 90°C tests reused the still-clear solution from the 30°C tests.) About 7.5×5.0 cm of surface area was anodized during each test. During these tests, the electrolyte was not previously saturated with iron.

The anodized steel surface was modified using different treatments. The boiled surface was boiled in pure water for 20 min. The oxidized surface was heated in air at 200°C for 30 min. Octadecyl phosphonic acid (ODPA) coatings were deposited on the anodized steel by first immersing the steel for 24 h in 5 mM ODPA dissolved in tetrahydrofurane (THF), next rinsing with THF, and then drying/curing the ODPA film at 70°C for several days in an air atmosphere. The Octadecyl silane (ODS) coatings were prepared by immersing

the steel for 19 h in 10 mM ODS dissolved in toluene, next rinsing with toluene, and then drying/curing for one day at 70°C in an air atmosphere. The oils (including WD-40 oil) were prepared by completely wetting the sample with the oil for 30 s and then immediately blowing the excess oil off the surface with compressed air at a low glancing angle. WD-40 is a commercial, water displacing, corrosion inhibitor and lubricant manufactured by WD-40 Company, San Diego, California. For the water-drop contact angle, the bare steel was prepared by polishing with 600 grit SiC, cleaning with cotton soaked first with acetone, then ethanol, and drying under a warm airstream.

The XRD measurements were conducted on a Philips X'Pert MPD System with the X-ray beam at a 1° incident angle to the sample. The scanning electron microscopy images were taken with a Hitachi S-4800 FESEM. For the cross sections, the steel samples were mounted on edge in epoxy and polished to 1 μm diamond paste, then etched for 30 s in 2% Nitol (2% nitric acid dissolved in ethanol), demagnetized, and either carbon coated or gold coated for electrical conductivity. The crimped steel samples were bent 180° to fracture the surface oxide.

The electrochemical voltammograms were conducted in deaerated, borate buffer solution with pH = 8.5. The borate solution contained 18.55 g H_3BO_3, 26.60 g $Na_2B_4O_7 \cdot 10H_2O$ dissolved in 1 L deionized (DI) water. The solution was deaerated prior to the voltammetry by bubbling with nitrogen gas. The electrochemical impedance spectroscopy (EIS) tests were conducted in an oxygenated 0.1% NaCl solution, saturated by bubbling oxygen gas prior to the tests, and the amplitude of the sine wave was 5 mV. The EIS test frequencies were from 10 kHz to 10 mHz, and each test took ~35 min.

Results and Discussion

Anodic oxide formation.— During preliminary experiments, the steel was anodized under many different conditions in various electrolytes. It was observed that the anodic oxide growth rate (in nanometers per second) on the steel was a function of several parameters. In general, the important parameters were the following:

1. Applied potential (voltage): higher voltages increased the rate (to a limit).
2. Temperature: hotter electrolytes increased the rate.
3. Concentration of the NaOH or KOH: more concentrated increased the rate.
4. Age (saturation) of the electrolyte: greater saturation increased the rate.
5. Potential-temperature region: different oxides grew at different rates.
6. Thickness of the oxide: after a time, thicker oxides grew at a faster rate.
7. Steel composition: the rate depended on the steel alloy composition.

Some of the data for these observations have been previously reported,[1] and some of the data are shown in the coming sections. Notably, the age (or the saturation) of the electrolyte was found to be a very important parameter. Initially, the solution was clear, but as the electric current passed through the steel, oxygen bubbles formed and swirls of pink or violet color could be seen forming in the solution near the steel anode. The pink-violet colors are indicative of ferrate (FeO_4^{-2}) production.[7,15] During the anodization process, the originally clear solution turned violet, and then a dark purple color.[1] The dark purple solutions grew the oxides at least 50% faster than the fresh clear NaOH. For a given time, potential, and temperature, the anodic oxide was not reproducible from sample to sample until the electrolyte was sufficiently aged, most likely saturated in ferrate anions (FeO_4^{-2}).

Figure 1 shows an oxide morphology map for steel anodized in 50% NaOH for 5 min at 7 cm spacing from the steel counter electrode. (These electrolytes were not saturated.) The different regions that were observed were the passive, dichroic, black adherent, and light brown oxides. The oxide regions are labeled according to their optical properties and their adherency. The adherent oxides are so named because they would not discolor when rubbed with a cotton swab nor would they lift off when adhesive tape was stuck to their surface and peeled off. The semiadherent oxides would be discolored by rubbing and would also show a brown stain on the cotton swab and on the clear adhesive tape. The top of Fig. 1 shows the approximate potential vs the Ag_2O/20% KOH reference electrode. It can be seen that both a minimum potential and temperature are required for visible oxide growth. In addition, the appearance of the oxide is highly dependent on both parameters.

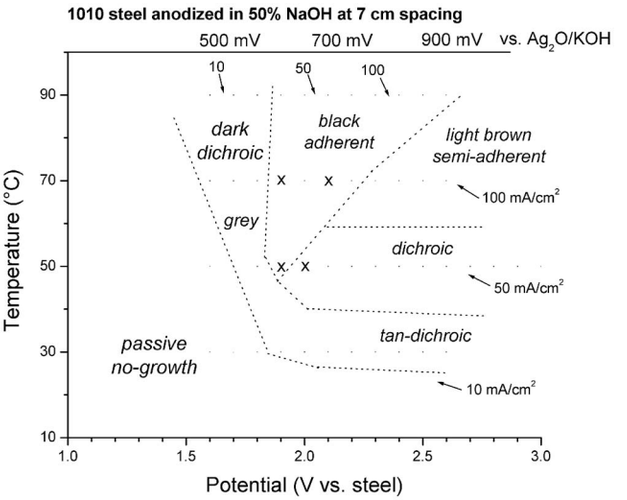

Figure 1. Optical and physical properties of the anodic oxide after being polarized for 5 min in 50% NaOH at different potentials and temperatures.

Figure 2 shows an oxide color map, with photographs of the steel and their potential vs the Ag_2O/KOH reference electrode. The different regions in Fig. 1 correspond to the different shades in Fig. 2. The current density shows a steady increase from almost zero in the passive region at the lower left corner, reaching 100 mA/cm^2 at the upper right corner. Too low of a temperature or potential results in no growth.

Morphology of the oxide layers.— The anodized films grew to a very uniform thickness across the surface. Figure 3 shows as an

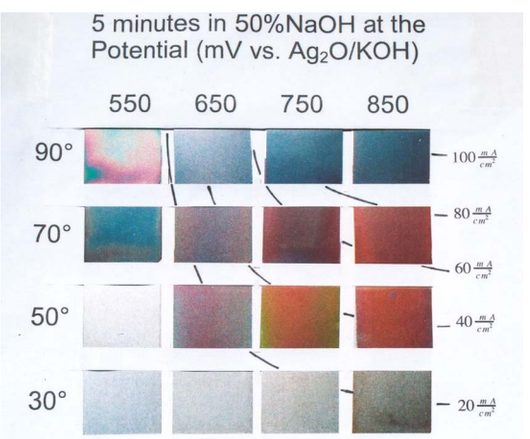

Figure 2. (Color online) Steel panels anodized in the 50% NaOH vs the Ag_2O/KOH electrode.

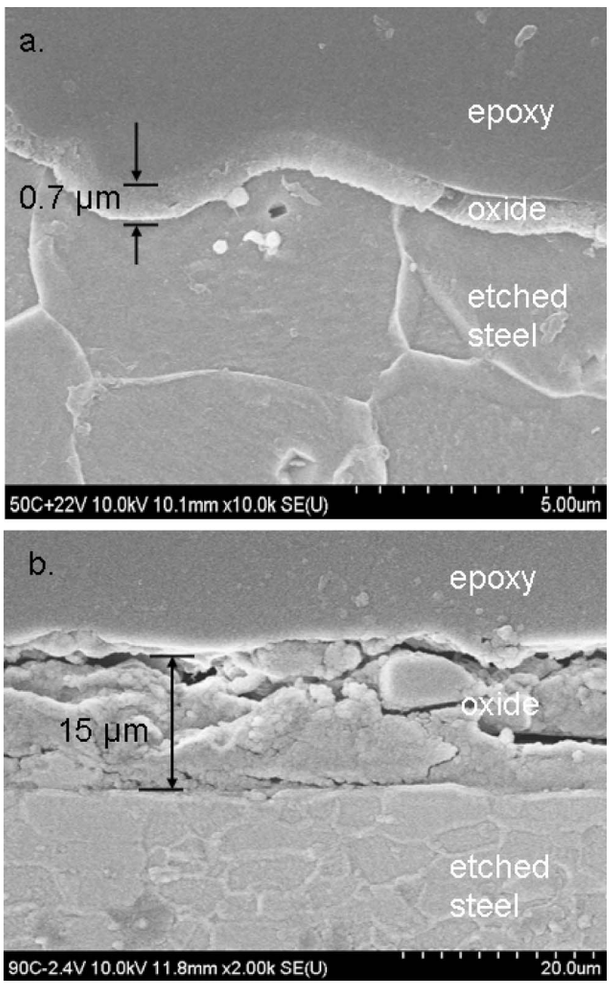

Figure 3. FESEM cross sections of the oxide film on steel grown at different temperatures and potentials: (a) 50°C, +2.2 V, and (b) 90°C, +2.4 V.

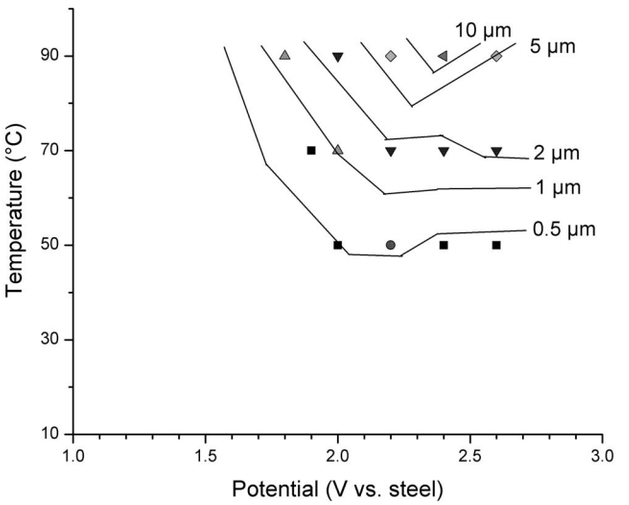

Figure 4. Thickness of the anodic oxides as measured from the FESEM cross sections.

example typical FESEM cross sections of the anodized steel for 50 and 90°C. For these images, the steel cross section was etched in 2% Nitol after polishing. At all temperatures, the oxide was uniform across the surface (Fig. 3a) and increased in thickness with increasing time, temperature, and voltage. In this set of samples, the thickest oxide was formed at 90°C, +2.4 V, but this oxide shattered during the mounting and polishing process (Fig. 3b) and does not appear as structurally stable as the thinner oxides.

The thicknesses as measured from the FESEM cross sections for all the panels are shown in Fig. 4. Increasing the temperature resulted in a thicker oxide after 5 min, and the increase in potential also increased the oxide thickness, but only up to a limit. At each temperature, there seems to be a limiting thickness under these experimental conditions and potential range. During the anodization, part of the electric current caused oxygen evolution, part caused steel dissolution, and part caused oxide growth. The discussion below shows that more of the electric current went for steel dissolution or oxygen evolution at the higher potentials.

The charge, which was consumed after 5 min of anodization, was recorded and used to calculate the oxide growth efficiency. If one assumed that all of the charge was used to grow a solid magnetite oxide film, then an ideal thickness could be calculated. The basis for calculating the ideal thickness T is shown as follows

$$T = \frac{QM}{AencN\rho} \quad [1]$$

In Eq. 1, Q is the electric charge passed (in amperes per minute), M is the atomic weight of Fe_3O_4 (231.6 g/mol), A is the surface area (in centimeters squared), e is the charge of an electron (1.602×10^{-19} coul), n is the number of electrons per Fe atom (2.667), c is the number of Fe atoms per Fe_3O_4 molecule (3), N is Avogadro's number (6.022×10^{23} atoms/mole), and ρ is the density of Fe_3O_4 (5.18 g/cm^3). After multiplying the constants and converting the units, Eq. 2 is obtained, where the ideal thickness T is in nanometers if charge Q is in amperes per minute and area A is in centimeters squared

$$T = \frac{Q}{A} \times 34{,}700 \quad [2]$$

Dividing the FESEM measured thickness of the oxide by the ideal oxide thickness T would give the percent efficiency of the oxide film formation. These calculations were repeated for each sample, and the following results were obtained: At 50°C, the oxide growth was ~25% efficient at +2.0 V, but decreased to ~5% efficient by +2.6 V. At 70°C, the oxide growth was ~40% efficient at +2.0 V, but decreased to ~10% by +2.6 V. At 90°C, the oxide growth was ~20 to ~40% efficient, peaking at ~70% efficient for +2.4 V. In general, the oxide growth was more efficient at the higher temperatures and the black adherent oxide was more efficient at growth than the dichroic oxide. However, these calculated efficiencies are exaggerated by four or five times, since they assume a solid magnetite layer was formed, not a porous oxide, as will be shown in the next section. In spite of this limitation, it can be seen that as the potential increased, less of the current went into oxide growth and more of the current went into iron dissolution and oxygen evolution.

The FESEM top view images of the anodized cold-rolled steel surface are shown in Fig. 5-8. Figure 5 is a top view of the dichroic (50°C, +2.0 V) anodized surface, and it shows a uniform porosity across the surface, with deeper attack along the grain boundaries (Fig. 5a). The opening of the pores on the top surface (Fig. 5b) was 20–40 nm diam.

The dichroic sample in Fig. 5 was next crimped 180° to fracture the oxide, and the FESEM images of the fractured surface oxide are shown in Fig. 6. The oxide cracking changed from grain to grain, depending on the local plastic deformation of the underlying steel crystal/grain (Fig. 6a). The grain boundaries are visible due to their

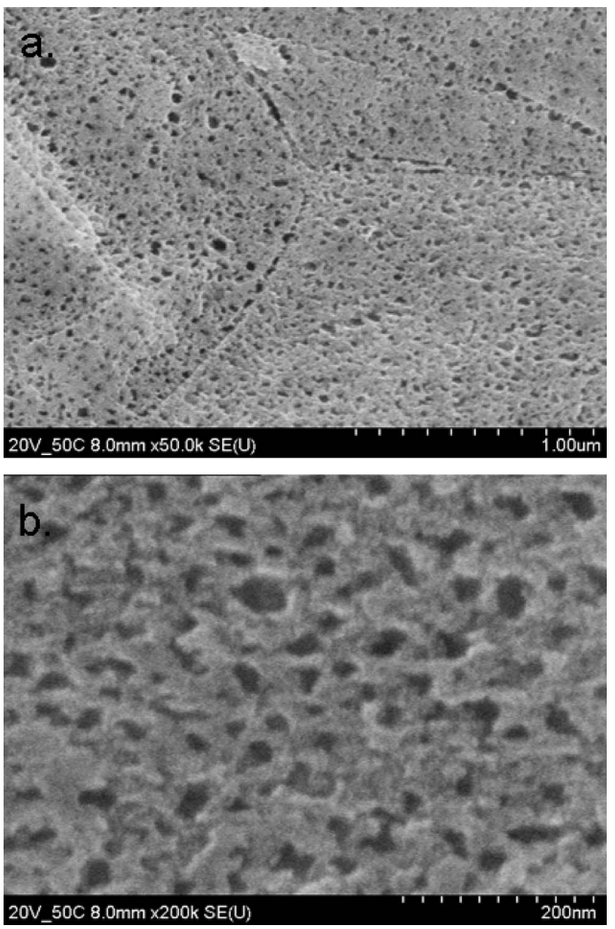

Figure 5. FESEM top view of dichroic oxide grown at 50°C, +2.0 V.

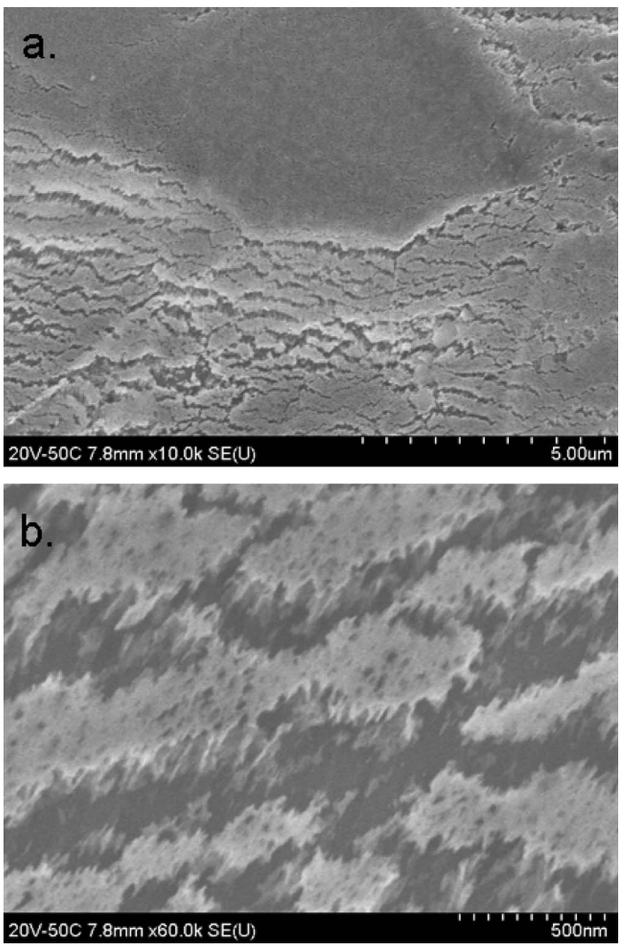

Figure 6. The same dichroic oxide as Fig. 5 (50°C, +2.0 V) except that the steel has been crimped to fracture the oxide. The oxide is very adherent to the underlying steel.

differences in deformation. The anodic oxide is thin and brittle, but it is adherent to the underlying metal even as the metal plastically deforms (Fig. 6b).

The appearance of the anodized film also varies across the surface, depending on the crystal orientation of the underlying steel grains. Figure 7 shows the FESEM top view of steel anodized at 70°C, +1.9 V (black adherent). The different grains of the steel substrate are readily visible by their different color shades after the anodizing (Fig. 7a). Higher magnification shows two adjacent grains where the lower grain has more open pores, while the upper grain has more closed-top pores (Fig. 7b). The grains were etched/anodized differently due to their different crystal orientations.

The thicker anodic oxides were also fractured by crimping the steel sheet. Figure 8 shows the fractured cross section of the anodic oxide grown at 70°C and +2.5 V (light brown semiadherent). The oxide has grown to 1 μm in thickness in 5 min (Fig. 8a). The small 20 nm diam pores on the top are connected to the long, hollow channels, which are ~100 nm diam, and extend the entire oxide thickness, from the top pores to the lower steel substrate. Figure 8b shows a portion of the oxide that had broken off and turned over. The broken channel walls are only 10–20 nm in thickness. Regardless of their optical appearance or their adherency, all the FESEM microstructures in Fig. 5-8 were remarkably similar with the only difference being different total oxide thicknesses and different size pore openings on the top surface.

Figure 9 shows the cross-sectional thickness (50°C, dichroic) as measured from the FESEM cross sections (solid line) and compared to the thickness as estimated from the color of the film (dashed or dotted lines). If the film is assumed to be solid magnetite, which has a refractive index $n = 2.42$, then the estimated thickness from the color (lower curve) is only half the thickness as that measured by the FESEM. However, if the layer between the top and the bottom of the film is assumed to be an air gap, with $n = 1.0$, then there is better agreement between the FESEM measurements and the thickness estimated from the color. This observation supports the concept that the dry anodic film is mostly air-filled, hollow channels. The thickness based on the color should therefore be 2.4× thicker than that previously calculated. The color-thickness relationships in Fig. 4 and in Table II in the Burleigh's previous work[1] should be replaced with the corrected Table I. In a similar fashion, filling these air-filled channels with liquids with different refractive indexes would change the color of the film.

On the basis of the above findings, we can address the film growth mechanisms in more detail. Figure 10 shows an idealized schematic of the anodic oxide. Ferrate anions (FeO_4^{-2}) are present in the aged electrolyte, as evidenced by the dark violet/purple color.[7,15] In experiments that began with the clear solutions, the violet color of the ferrates was more intense a few millimeters distant from the steel anode, indicating that the iron dissolved initially as Fe^{+6} and then reacted with the hydroxyls in the solution to form the ferrate via the reaction shown in Eq. 3. Also at the steel anode surface, oxygen evolution is occurring as evidenced by the bubbling. Typical oxygen evolution reactions (OERs) would consume hydroxyls (Eq. 4) or produce hydrogen cations (Eq. 5), both of which would result in a lower pH adjacent to the anode interface vs the bulk solution

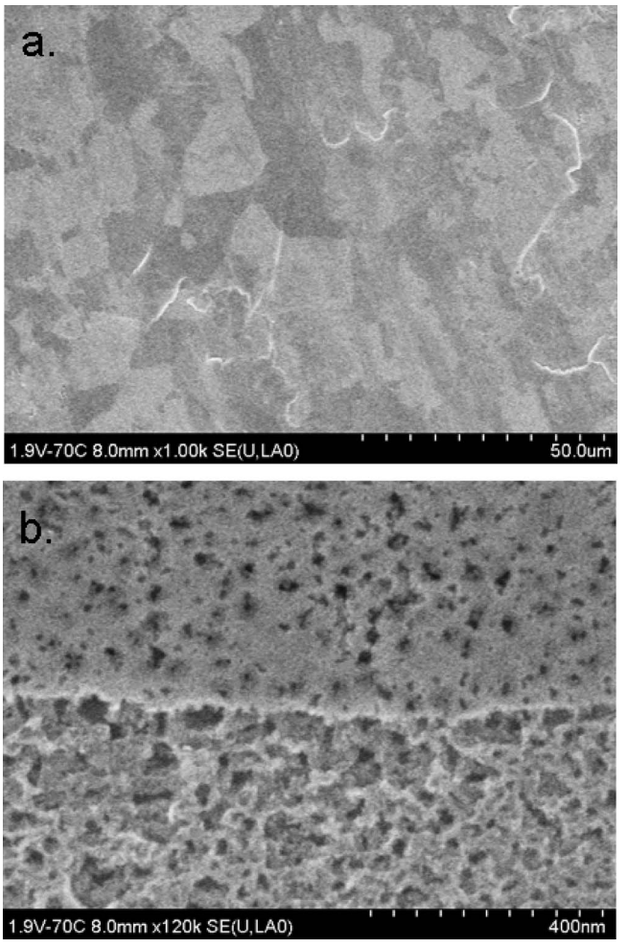

Figure 7. FESEM top view of black oxide anodized at 70°C, +1.9 V. The different grains are anodized/etched differently.

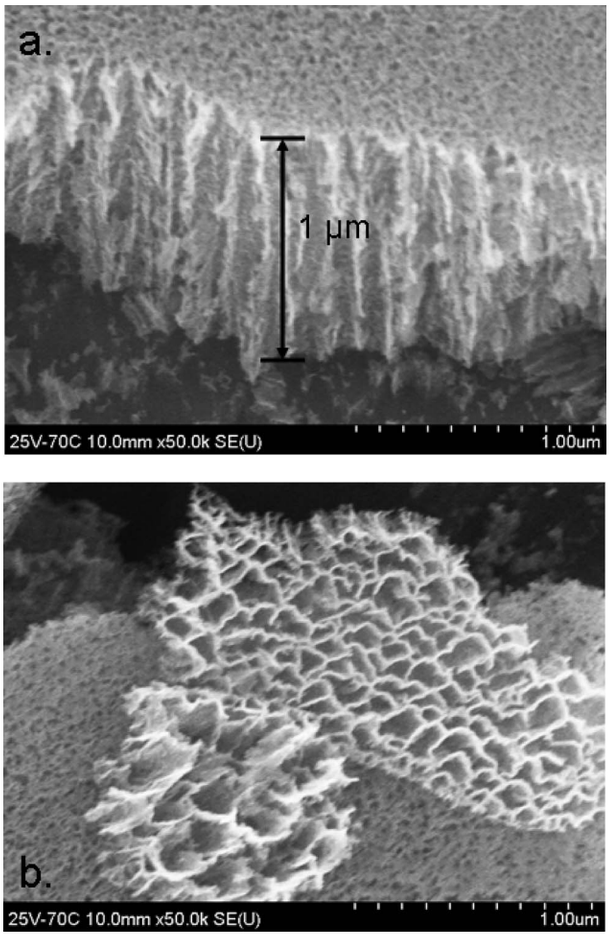

Figure 8. FESEM of the fractured oxide (70°C, +2.5 V) showing (a) the nanoporous hollow channels and (b) the inside of an upside-down section of the channels.

$$Fe^{+6} + 8OH^- \rightarrow FeO_4^{-2} + 4H_2O \quad [3]$$

$$4OH^- \rightarrow 4e^- + 2H_2O + O_2 \quad [4]$$

$$2H_2O \rightarrow 4e^- + 4H^+ + O_2 \quad [5]$$

Speculating on the mechanism of formation of the anodic oxide film, two possible mechanisms could be operative, namely, (a) the dissolution-precipitation mechanism, by which steel typically rusts in fresh water (e.g., Ref. 16), or (b) the flow mechanism of pore generation, by which the porous anodic oxide grows on aluminum.[17] For the dissolution-precipitation mechanism, the negatively charged ferrate in the solution would be attracted back to positive steel anode and precipitate out of the solution on the steel anode as magnetite (Fe_3O_4), via Eq. 6 or 7. The precipitation of magnetite would also result in oxygen evolution, and Eq. 6 would require the electrical conductivity of the magnetite to transport the excess electrons back to the positively charged steel base metal. In the alternative Eq. 7, the ferrate would combine with hydrogen cations to precipitate Fe_3O_4, but there would be no electron transport to the base metal

$$3FeO_4^{-2} \rightarrow Fe_3O_4 + 4O_2 + 6e^- \quad [6]$$

$$3FeO_4^{-2} + 6H^+ \rightarrow Fe_3O_4 + 4O_2 + 3H_2O \quad [7]$$

The second possible mechanism, the flow mechanism of pore generation,[17] would explain the uniform thickness of the anodic oxides shown in Fig. 3, 5, and 8. On the basis of this mechanism, the iron would first oxidize to Fe^{+2} and Fe^{+3} and form magnetite, Fe_3O_{4c}, at the metal interface. Further oxidation of the magnetite at the electrolyte interface would form the soluble Fe^{+6}. The magnetite layer would plastically flow by electrostriction stresses and would

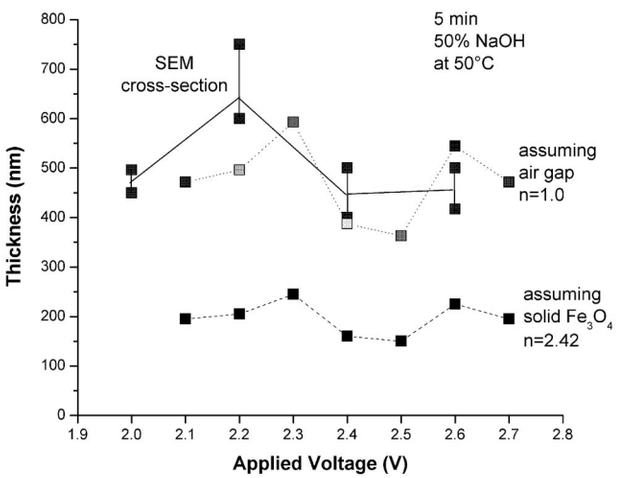

Figure 9. Oxide thickness as determined from the FESEM cross sections and estimated from the color of the film assuming different refractive indexes, *n*.

Table I. Thickness of the dichroic film as estimated from its color, by comparing to silica on silicon (Ref. 18). Optical thickness = $n_0t_0 = n_1t_1$.

Film thickness (nm) for thermally grown SiO_2 $n = 1.46$	Color as viewed from directly above Silica data from Pliskin and Conrad[18]	Film thickness (nm) for air-filled channels $n = 1.0$	Film thickness (nm) for solid magnetite $n = 2.42$
50	Tan	**75**	30
70	Brown	**110**	40
100	Dark violet to red violet	**145**	60
120	Royal blue	**175**	70
150	Light blue to metallic blue	**220**	90
170	Metallic to very light yellow green	**250**	100
200	Light gold or yellow slight metallic	**290**	120
220	Gold with slight yellow-orange	**320**	130
250	Orange to melon	**365**	150
270	Red-violet	**395**	160
300	Blue to violet-blue	**440**	180
310	Blue	**450**	190
320	Blue to blue-green	**465**	195
340	Light green	**495**	205
350	Green to yellow-green	**510**	210
370	Green-yellow	**540**	225
390	Yellow	**570**	235
410	Light orange	**600**	245
420	Carnation pink	**615**	255
440	Violet-red	**640**	265
460	Red-violet	**670**	280
470	Violet	**685**	285
480	Blue-violet	**700**	290
490	Blue	**715**	295
500	Blue-green	**730**	300

be squeezed up from the base of the pores to form the thin, 10–20 nm thick channel walls. This mechanism has been described by Skeldon et al.[17] to explain the formation of porous aluminum oxide and the uniform thickness of the oxide layer. The flow mechanism could also explain the different appearance of the anodic oxide over the grain boundaries (Fig. 5a) and over the different grains (Fig. 7), since a solid-state reaction would have a crystallographic relationship between the base metal and the oxide. Precipitation is generally less uniform and less dependent on the crystallographic orientation of the base metal and the presence of grain boundaries. It is possible however that both mechanisms play a role in the oxide growth, initially growing via the flow mechanism for the adherent oxides, and then changing to the precipitation mechanism for the very thick, nonadherent oxides.

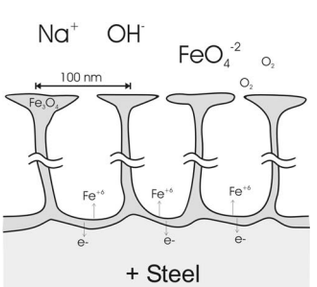

Figure 10. Schematic of the nanoporous magnetite (Fe_3O_4) channels that compose the anodic oxide.

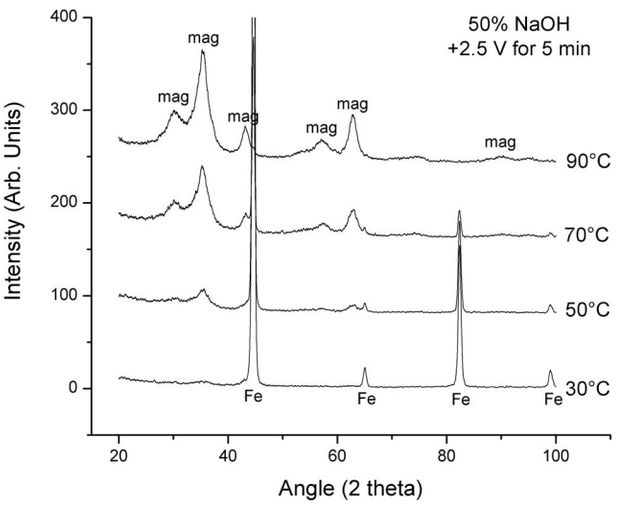

Figure 11. Thin-film XRD and the effect of temperature on the anodic oxides.

Characterization with XRD.— The crystal structure of the anodic oxide films was studied with glancing angle XRD. Figures 11 and 12 show the thin film XRD results for steel anodized at +2.5 V and at four different temperatures. At this applied voltage, the film changes from tan-dichroic at 30°, to dichroic at 50°, to light brown at 70°, to black at 90°. Only the XRD peaks for magnetite and iron are visible in Fig. 11. As the temperature increases, the size of the magnetite peaks increase, and by 90°C, the film is thick enough to completely mask the underlying Fe substrate. These magnetite peaks are relatively broad, indicating that the average crystal size is very small. Using the magnetite peak broadening and the Scherrer formula,[19] the average crystal size of the magnetite was calculated to be 4–5 nm. The reason the peaks were postulated to be magnetite rather than maghemite is explained in the next paragraph.

The X-ray peaks at 2θ angle of 90 and 95°, along with the positions for magnetite (cubic-Fe_3O_4) and maghemite (γ^3–Fe_2O_3) are shown in Fig. 12. These broad peaks could match either of these two oxides. Because magnetite is the black-colored iron oxide,[16] and because the multiple fine-structure lines, which should be present for the maghemite are absent, we postulate that the films are primarily magnetite (Fe_3O_4), which is in agreement with previous results.[1]

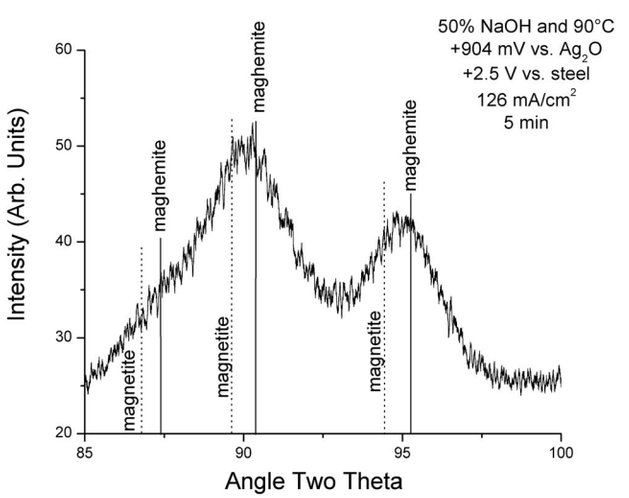

Figure 12. Thin film XRD of the high angle peaks.

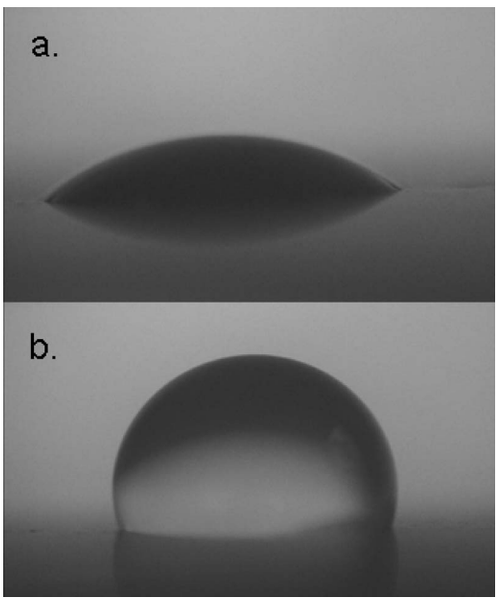

Figure 13. Water drops on anodized steel (70°C, +2.5 V): (a) untreated and (b) coated with ODPA.

However, the film could also be a multilayer oxide, since magnetite and maghemite have the same cubic crystal, only differing amounts of oxygen. The inner layer would be magnetite with a lower percentage oxygen, and the outer layer would be maghemite with more oxygen. The light brown semiadherent oxide could contain more maghemite because it also has a reddish-brown color.[16]

The XRD data is in good agreement with results from the preliminary XPS studies. The oxide layers formed at 50 and 70°C contained iron and oxygen in a ratio consistent with Fe_3O_4. However, the oxide layers formed at 90°C contained slightly higher oxygen, more in line with Fe_2O_3. Additional XPS characterization is required to confirm these preliminary trends and their significance.

Water drop contact angles.— Another property of the oxide film is the water drop contact angle, which gives a measure of the hydrophilic or hydrophobic nature of the surface. Figure 13 shows water drops on steel anodized at 70°C and +2.5 V (light brown, semiadherent oxide). The anodized steel is hydrophilic, as seen by the low contact angle on anodized steel (Fig. 13a). In order to change the wetting properties of the surface oxide, the anodic film was coated with different organic compounds. For example, if the same anodized steel is coated with ODPA, it becomes hydrophobic (Fig. 13b).

Several different surface treatments were used to alter the hydrophobicity of the anodized surface. A summary graph of the water-drop contact angles after different treatments is shown in Fig. 14. The dashed line in the center of the graph is the contact angle for bare steel, which has a contact angle of 72°. The anodized steel with no surface treatment had the lowest water-drop contact angle (25°), whether or not it was coated with WD-40. Boiling or steaming the anodized steel in pure water slightly increased the water-drop contact angle (~50°). Coating the anodized film with ODS or ODPA increased the water drop contact angle considerably (~100°). The water-drop contact angle on the ODPA-coated anodic layer is fairly independent of the temperature or potential at which the surface was anodized. Although the different surface treatments change the water-drop contact angle, there was no direct relationship observed between the water drop contact angle and the corrosion resistance, as will be shown in the next section.

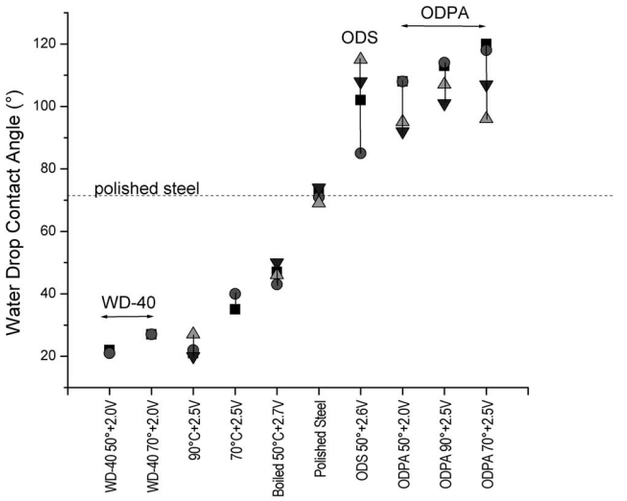

Figure 14. Water-drop contact angles of the anodized steel with different treatments.

Electrochemistry and corrosion testing.— The anodic film on steel was characterized using electrochemical techniques. Figure 15 compares the steady-state voltammograms (after 10 cycles) of the anodized film vs polished steel in deaerated borate-buffer solution cycled at 50 mV/s. In the borate buffer solution, bare steel was passive, as seen by the very low currents. The anodic films however have much larger current densities in both the anodic and cathodic directions. The magnitude of the current density was larger as the anodic film became thicker. The 4.5 μm thick film (90°C, +2.2 V) has twice the current density of the thinner 1.1 μm thick film (70°C, +2.0 V). The anodized film consists of a porous network of magnetite (Fe_3O_4) channels that apparently absorb charge as the oxide switches between Fe^{+2} and Fe^{+3}. Similar switching between Fe^{+2} and Fe^{+3} has been shown previously for iron in KOH solutions.[20] Calculations of the charge in each current loop in Fig. 15 show that only ~20% of the available porous oxide actually participates in the anodic-cathodic switching.

Steel has been reported to corrode in distilled water at room temperature at 1570 g/m^2/day,[21] which is equivalent to 73 mm/yr. If drops of pure water were placed on polished or cold-rolled steel,

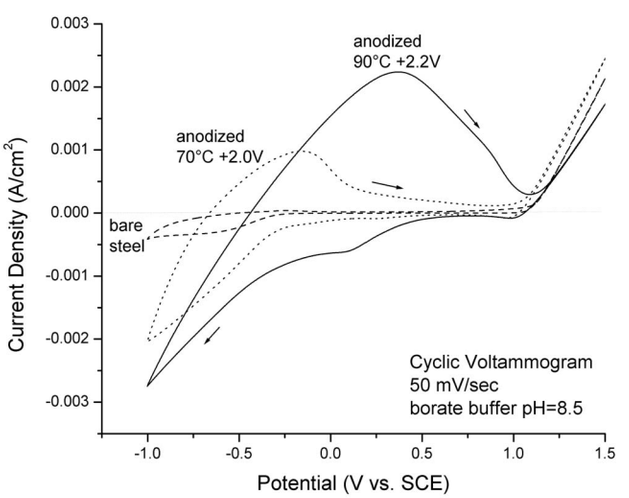

Figure 15. Voltammogram of the anodized steel vs bare steel in borate-buffer solution.

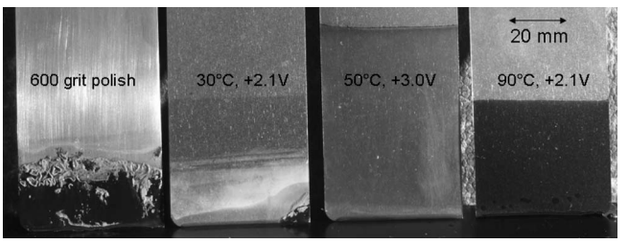

Figure 16. Appearance of the steel samples after 10 days partial immersion in 100 mL pure water (18 MΩ cm) open to the atmosphere. Panels are still wet in this photograph.

then a rust spot remained after the water had evaporated. However, when pure water drops were placed on the anodized steel, there was no visible trace remaining after the water had evaporated. In addition, simple immersion tests were also conducted with the anodized steel. The panels were partially immersed in beakers of pure water that were open to the atmosphere. The pure water was 100 mL of DI 18 MΩ cm water, in 250 mL beakers, so that only the lower 30 mm of each panel was exposed. Figure 16 shows that after 10 days, the 600 grit polished steel was very rusted, and the steel anodized at 30°C and +2.1 V had rust beginning at the lower right corner. However, the steel panels anodized at the higher temperatures, (50, 70, and 90°C) and >2.0 V, showed no corrosion in the pure water open to air, even four weeks later when the water had completely evaporated.

The anodized steel, which showed excellent corrosion resistance to pure water, had only temporary resistance to oxygenated saltwater. If the steel anodized at +2.5 V and 50, 70, and 90°C was coated with ODPA, it showed better resistance to corrosion by the saltwater drops, but this protection was temporary. Often the ODPA-coated steel exhibited rusting when the saltwater drops had evaporated.

EIS was used to measure the corrosion rates of the steel samples in oxygenated saltwater (0.1% NaCl saturated with O_2). The samples were allowed to freely corrode in the saltwater for a given time, and then they were polarized to −500 mV vs saturated calomel electrode (SCE) for testing with EIS. The −500 mV SCE was used as the test potential because the individual open-circuit potentials (OCP) varied for the steel with the different coatings, and −500 mV SCE was approximately the OCP for freely corroding steel.

The Bode plots, shown in Fig. 17, compare the absolute impedance of polished bare steel to the anodized steel. (The phase angle,

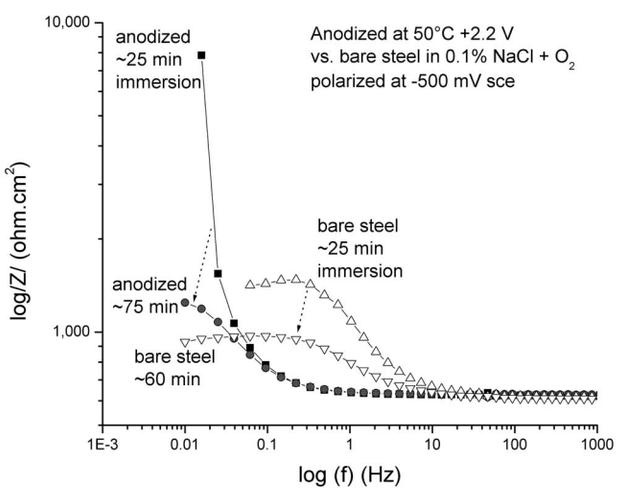

Figure 17. EIS of polished steel vs anodized steel in oxygenated 0.1% NaCl solution.

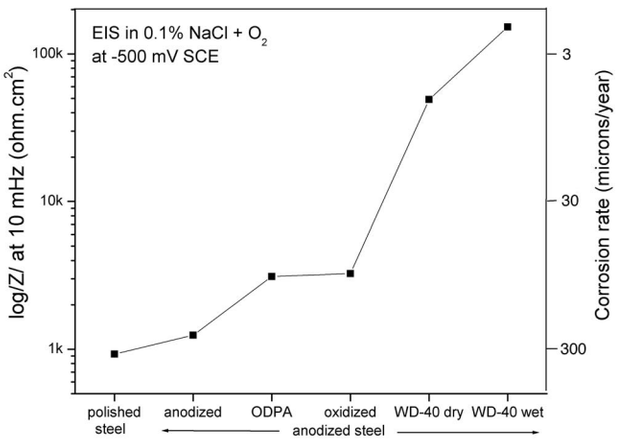

Figure 18. Corrosion rates with different coatings after 1 h immersion in oxygenated 0.1% NaCl.

not shown, follows the normal trends.) The polished bare steel (open triangles) in Fig. 17 shows very low impedance (and, thus, very little corrosion resistance) after ~25 min immersion in oxygenated saltwater, and even lower impedance after ~60 min. Initially, the anodized steel had a very high impedance (solid squares), but after ~75 min immersion the impedance dropped by 8× (solid circles). After 1 h in saltwater, the anodized steel had only a slightly higher polarization resistance than the uncoated bare steel. Noteworthy in these curves is that the impedance curve for the anodized steel has shifted to the left to much lower frequencies than the bare steel. This frequency shift is indicative of the much higher capacitance for the anodized layer due to the very large porous surface area of anodic oxide that is in contact with the electrolyte.

The anodized steel was boiled, steamed, oxidized, immersed in inhibitors, and coated with different organic compounds in order to seal the pores. These treatments generally only offered short-term corrosion protection, with the notable exception being that of the commercial oil spray WD-40. Figure 18 shows some of the results of the EIS tests. The left axis is the absolute impedance measured at 10 mHz after 1 h immersion in the solution. This absolute impedance corresponds to, approximately, the polarization resistance (R_p). By assuming B = 30 mV (see the calculations by Jones[22]), the estimated corrosion current may be calculated. This corrosion current was converted into an average corrosion rate,[22] and is shown on the right axis in Fig. 18. It may be seen that the corrosion rate of the steel was reduced 100× by anodizing and then sealing the pores with WD-40. It was also found that wet WD-40 is more protective than dry WD-40, and two coats were better than one.

The remarkable corrosion resistance provided by the anodized steel in combination with WD-40 is shown in Fig. 19. Here, the EIS tests in oxygenated saltwater are shown after spraying the steel with WD-40 and blowing off the excess. The most notable observation is that the vertical impedance scale is 20× larger than in Fig. 17. With WD-40, the anodized steel shows 100× higher polarization resistance, R_p. Even after three days immersion, the anodized steel still showed excellent corrosion resistance. In comparison, the lowest curve, which is for untreated anodized steel, shows poor corrosion resistance after only 1 h. Figure 19 also illustrates that the corrosion inhibition effect is not due only to WD-40. If polished steel is sprayed with WD-40, then its corrosion resistance is improved (middle curve), but it still has a 50× lower corrosion resistance than the anodized steel that was coated with WD-40. The authors hypothesize that WD-40 is entering and sealing the pores in the magnetite film.

The above results have demonstrated the multifunctional properties of the anodized oxide films on steel. Possible service applications for this anodization process on steel include transit rust pro-

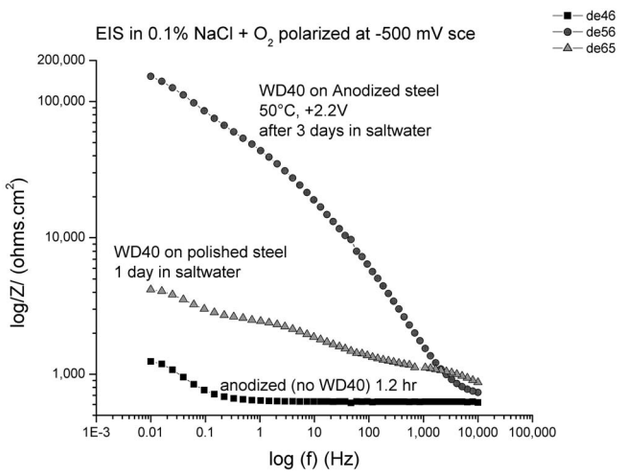

Figure 19. EIS in oxygenated 0.1% NaCl solution with and without spraying the anodized film with WD-40.

tection or serving as conversion coatings for paints or reservoirs for holding inhibitors and oils or a preweathering process for the weathering steels. Postulated mechanisms for the formation of the anodic oxide and also an effective method for sealing the pores have been described.

Conclusion

The anodic oxide film grown on steel in hot caustic solution has many remarkable multifunctional properties. Optically, the appearance of the oxide varies from black to dichroic to a light brown color, but the microstructure and the crystallography are similar for the different regions. The dichroic oxide has the colors of the rainbow, depending on the optical thickness. The oxide was examined with FESEM, XRD, and electrochemical methods. FESEM and XRD revealed the oxide to be a nanoporous oxide composed of a network of thin-walled magnetite channels. Electrochemically the oxide is a very good conductor and, when polarized, can partially switch between Fe^{+2} and Fe^{+3}. The corrosion resistance of the anodic films was investigated, and although the film provides excellent resistance to pure water, it does corrode in oxygenated saltwater. Various methods were used to seal the pores of the oxide, and it was found possible to increase the corrosion resistance in saltwater by over 100 times by spraying the anodized surface with a commercial corrosion inhibitor WD-40, which apparently penetrated into the pores.

Acknowledgments

T.D.B. appreciates the funding he received from the Alexander von Humboldt Foundation, the Lehrstuhl für Korrosion und Oberfläche at Universität-Erlangen-Nürnberg, the National Science Foundation grant no. EPS 0312632, and the New Mexico Tech Office of Academic Affairs. We thank Evan Prichard, Inge Tontsch, Uli Marten, Helga Hildebrand, Hans Rollig, Martin Kolacyak, and Anja Friedrich for their valuable assistance.

New Mexico Tech assisted in meeting the publication costs of this article.

References

1. T. D. Burleigh, T. C. Dotson, K. T. Dotson, S. J. Gabay, T. Sloan, and S. G. Ferrell, *J. Electrochem. Soc.*, **154**, C579 (2007).
2. D. D. MacDonald and B. Roberts, *Electrochim. Acta*, **21**, 557 (1978).
3. R. S. Schrebler Guzman, J. R. Vilche, and A. J. Arvia, *Electrochim. Acta*, **24**, 395 (1979).
4. W. C. He, H. B. Shao, Q. Q. Chen, J. M. Wang, and J. Q. Zhang, *Acta Phys.-Chim. Sin.*, **23**, 1525 (2007).
5. S. Joiret, M. Keddam, X. R. Novoa, M. C. Perez, C. Rangel, and H. Takenouti, *Cem. Concr. Compos.*, **24**, 7 (2002).
6. A. Costine, S. Thurgate, M. Thornber, and C. Vernon, *Surf. Interface Anal.*, **39**, 452 (2007).
7. F. Beck, R. Kaus, and M. Oberst, *Electrochim. Acta*, **30**, 173 (1985).
8. K. Bouzek, I. Rousar, H. Bergmann, and K. Hertwig, *J. Electroanal. Chem.*, **425**, 125 (1997).
9. M. Koltypin, S. Licht, R. T. Vered, V. Nashits, and D. Aurbach, *J. Power Sources*, **146**, 723 (2005).
10. J. F. Jackovitz and G. A. Bayles, in *Handbook of Batteries*, 2nd ed., D. Linden, Editor, p. 30.1, McGraw-Hill (1995).
11. H. L. Hollis, U.S. Pat. 621084 (1899).
12. H. L. Hollis, U.S. Pat. 664550 (1900).
13. H. L. Hollis, U.S. Pat. 827802 (1905).
14. J. A. McCarthy, U.S. Pat. 3275536 (1966).
15. M. Pourbaix, *Atlas of Electrochemical Equilibria in Aqueous Solutions*, p. 644, NACE Cebelcor, Houston (1974).
16. R. M. Cornell and U. Schertmann, *The Iron Oxides*, VCH, Weinheim (1996).
17. P. Skeldon, G. E. Thompson, S. J. Garcia-Vergara, L. Iglesias-Rubianes, and C. E. Blanco-Pinzon, *Electrochem. Solid-State Lett.*, **9**, B47 (2006).
18. W. A. Pliskin and E. E. Conrad, *IBM J. Res. Dev.*, **8**, 43 (1964).
19. B. D. Cullity and S. R. Stock, *Elements of X-Ray Diffraction*, 3rd ed., Prentice-Hall, Englewood Cliffs, NJ (2001).
20. P. Schmuki, M. Büchler, S. Virtanen, H. S. Isaacs, M. P. Ryan, and H. Böhni, *J. Electrochem. Soc.*, **146**, 2097 (1999).
21. E. Rabald, *Corrosion Guide*, 2nd rev. ed., p. 882, Elsevier, Amsterdam (1968).
22. D. A. Jones, *Principles and Prevention of Corrosion*, 2nd ed., p. 148 and p. 72, Prentice-Hall, Englewood Cliffs, NJ (1996).